Developing a distributed modeling framework considering the spatiotemporally varying hydrological processes for sub-daily flood forecasting in semi-humid and semi-arid watersheds

Xiaoyang Li
Dalian University of Technology
Lei Ye (yelei@dlut.edu.cn)
Dalian University of Technology
Xuezhi Gu
Dalian University of Technology
Jinggang Chu
Dalian University of Technology
Jin Wang
Hubei Key laboratory of Intelligent Yangtze and Hydroelectric Science
Chi Zhang
Dalian University of Technology
Huicheng Zhou
Dalian University of Technology

Research Article

Keywords: Semi-arid and semi-humid watersheds, Distributed hydrological model, Sub-daily Flood forecasting, Flood event

Posted Date: January 25th, 2024

DOI: https://doi.org/10.21203/rs.3.rs-3870445/v1

Developing a distributed modeling framework considering the spatiotemporally varying hydrological processes for sub-daily flood forecasting in semi-humid and semi-arid watersheds

Xiaoyang Li[1], Lei Ye[1,*], Xuezhi Gu[1], Jinggang Chu[1], Jin Wang[2,3], Chi Zhang[1], Huicheng Zhou[1]

[1] School of Hydraulic Engineering, Dalian University of Technology, Dalian 116024, China

[2]China Yangtze Power Co., Ltd., Yichang, China

[3]Hubei Key Laboratory of Intelligent Yangtze and Hydroelectric Science, Yichang, China

Email address:

yelei@dlut.edu.cn

Corresponding author:

Name: Lei Ye

Complete postal address: School of Hydraulic Engineering, Dalian University of Technology, Dalian 116024, China

Abstract

The complex and varied climate, short duration and high intensity of rainfall, and complicated subsurface properties of semi-humid and semi-arid watersheds pose challenges for sub-daily flood forecasting. Previous studies revealed that lumped models are insufficient because they do not effectively account for the spatial variability of hydrological processes. Extending the lumped model to a distributed modeling framework is a reliable approach for runoff simulation. However, existing distributed models do not adequately characterize the strong spatiotemporal variability of the sub-daily hydrological processes in semi-humid and semi-arid watersheds. To address the above concerns, a distributed modeling framework was proposed that is extended by lumped models and accounts for the effects of time-varying rainfall intensity and reservoir regulation on hydrological processes. Moreover, the Fourier Amplitude Sensitivity Test (FAST) method is performed to identify the sensitive parameters for efficient calibration. To evaluate the performance of the proposed distributed model, it was tested in eight watersheds. The results indicate that the proposed distributed model simulates sub-daily flood events with mean evaluation metrics of 0.80, 9.2%, 13.0%, and 1.05 for NSE, BIAS, RPE, and PTE, respectively, superior to the lumped model. Furthermore, to further evaluate the difference between the proposed distributed model and the existing distributed models, it was compared with the Variable Infiltration Capacity (VIC) model at various time steps, including 3h, 6h, 12h, and24 h. The proposed distributed model was able to better capture the flooding processes at shorter time steps, especially 3 h. Therefore, it can be considered a practical tool for sub-daily flood forecasting in semi-humid and semi-arid watersheds.

Keywords: Semi-arid and semi-humid watersheds; Distributed hydrological model; Sub-daily Flood forecasting; Flood event

1 Introduction

Approximately 24% of the global land area is made up of semi-humid and semi-arid regions, with a population of more than 1.7 billion people (Zhang and Li, 1999; Granit, 2014). These areas are characterized by high rainfall intensities and short flood peak durations, resulting in frequent flooding and substantial loss of life and property (He et al., 2018; Khaing et al., 2019). To mitigate the impact of flooding on the risk regions, it is critical to develop effective hydrological models for flood forecasting, especially at finer time scales (Chang et al., 2019; Sivakumar and Singh, 2012). However, studies have discovered that most of the prevailing hydrological models do not perform up to par for sub-daily flood forecasting in semi-humid and semi-arid watersheds due to the unique hydrological characteristics and heterogeneous subsurface (Chao et al., 2019). Thus, developing hydrological modeling and flood forecasting techniques suitable for the hydrological characteristics of semi-humid and semi-arid watersheds remains an imperative task.

Hydrological models are commonly classified into lumped models and distributed models (Devia et al., 2015). The lumped models, which describe the watershed rainfall-runoff processes as a whole, are extensively utilized for daily and monthly runoff simulations with reasonable accuracy (Hapuarachchi et al., 2011). However, for sub-daily flood forecasting, the spatiotemporal variability of the hydrological processes is exceedingly intense and cannot be ignored. The performance of the lumped model is severely constrained because it is unable to adequately take into account the spatiotemporal variability of runoff generation and routing processes (Woods and Rowe, 1996). To overcome these limitations, extending lumped models into distributed models by allocating spatial characteristics, including rainfall, topography, and soil type, to different grid cells is a promising pathway (Yao et al., 2009).

Distributed models have been extensively applied to sub-daily flood simulation in humid watersheds with reasonable accuracy (Clark et al., 2011; Huo et al., 2020). This is because humid watersheds are characterized by sufficient rainfall and small soil water deficit, making distributed models effective in describing the spatiotemporal variability of hydrological processes (Werkhoven et al., 2008). Conversely, semi-humid and semi-arid watersheds are characterized by a complex and varied climate, short duration and high intensity of rainfall, leading to high non-linearity of hydrological processes (Wheater et al., 2007). Additionally, semi-humid and semi-arid watersheds usually experience a long period of drought and absence of rainfall preceding flooding, and reservoirs exhibit significant regulation effects on hydrological processes (Peng et al., 2017). Liu et al. (2020) proposed a hybrid runoff generation method applied to semi-humid and semi-arid watersheds without incorporating the effects of rainfall intensity and reservoirs, limiting the precision of the flood peaks simulation considerably. Similarly, Tian et al. (2020) simply developed the gridded Hebei model for semi-humid and semi-arid watersheds to explore appropriate scales for hydrological modeling, but it performed ineffectively in simulating flooding processes. To improve the applicability of the distributed model in semi-humid and semi-arid watersheds, the effects of rainfall intensity and reservoir regulation on runoff generation and routing processes inevitably need to be addressed.

Dramatic variations in rainfall intensity over time in semi-humid and semi-arid watersheds lead to flooding processes exhibiting strong non-linearity effects (Yi et al., 2022). The commonly used routing methods, including the diffusion wave, the kinematic wave method, and the horizontal routing (IRF-UH) method, only consider the spatial variability of rainfall while ignoring the effects of time-varying rainfall intensity on river routing (Lohmann et al., 1996; Zang et al., 2021). Lee et al. (2010) integrated a time-varying unit hydrograph of watersheds with a lumped model to account for time-varying rainfall intensities on flooding processes. Yi et al. (2022b) incorporated rainfall intensity into the SCS flow velocity formula based on a lumped model to improve the forecast accuracy of the watershed outlet. However, most of the existing studies are limited to lumped models, using only one time-varying unit hydrograph over the whole watershed, while distributed routing methods that consider the effects of rainfall intensity are uncommon (Paul et al., 2018). Therefore, it is worthwhile to explore a distributed routing method that is capable of handling time-varying rainfall intensity.

Numerous small and medium-sized reservoirs have been built to alleviate the shortage of water resources, and the regulation of reservoirs has severely altered the natural flooding processes (Payan et al., 2008a). The existing distributed models have developed different reservoir operating modules to simulate the regulation effects of reservoirs. For instance, Zhang et al. (2012) established the complex relationship between water surface area and storage of various types of reservoirs in the SWAT model based on the satellite dataset to simulate the variation of reservoir storage. Zhao et al. (2016) used a variety of observed operational data on reservoirs to calculate the storage and outflow of multi-purpose reservoirs in the DHSVM model. These reservoir modules are characterized by complex reservoir operating schemes driven by large amounts of real-time operational data. However, the reliance on real-time operational data makes it difficult to apply complex reservoir modules for sub-daily flood forecasting. Therefore, simplified reservoir modules that do not rely on real-time operational data in describing the regulation effects of reservoirs on flooding processes need to be explored.

To effectively tackle the strong spatiotemporal variability of hydrological processes in semi-humid and semi-arid watersheds, a distributed modeling framework extended by a lumped model is proposed. The distributed modeling framework accounts for the influences of the varying rainfall intensity and the regulation effects of small and medium-sized reservoirs to improve the capability of sub-daily flood forecasting. The main efforts of the present study are given as follows: (1) Extending the lumped model into a distributed modeling framework to fully account for the spatial heterogeneity of spatial characteristics. (2) Proposing a distributed river routing method that accounts for the time-varying rainfall intensity to tackle the issue of high non-linearity in the flooding processes. (3) Developing a reservoir module that describes the regulation effects of reservoirs on flooding processes without requiring real-time operational data.

This study is organized as follows: Section 2 describes the lumped model, the proposed distributed model, and the parameter calibration method. Section 3 presents the study area, data, and modeling process. Section 4 presents the comparison of the proposed distributed model with the lumped model and the VIC model. Finally, Section 5 provides the conclusion and perspective of this study.

2 Methodology

This study proposed the Grided-Dahuofang (GDHF) model, which was extended from the lumped Dahuofang (DHF) model. The lumped DHF model is widely used in semi-humid and semi-arid watersheds in northern China, especially for the Song-Liao Watershed in the Northeast (Meng et al., 2012; Yan et al., 2022). In this section, the mechanisms and structure of the lumped DHF model and the GDHF model are presented. Additionally, parameter sensitivity analysis and calibration methods are introduced.

2.1 The runoff generation module of lumped DHF model

The lumped DHF model was originally proposed in 1973 by the Dahuofang Reservoir Administration, China based on long-term forecasting experience (Liu and Wang, 1984). The lumped DHF model reasonably generalizes the rainfall-runoff process with a simple model structure and concise parameters. In the lumped DHF model, soil is generalized into three layers: the surface soil, lower soil, and deep soil, as shown in **Fig. 1(a)**. The surface soil layer describes the dynamics of soil moisture and surface water storage. S_a is the sum of the water stored in the surface soil layer and the water retained by vegetation interception and depression detention. The lower soil layer reflects the dynamic effect of rainfall processes on runoff generation, and U_a represents the water storage in this layer. V_a denotes the water storage of the deep soil layer. S_0, U_0, and V_0 are the water storage capacities of the surface soil, lower soil, and deep soil, respectively. The lumped DHF model adopted the two-layer infiltration curve to account for heterogeneity in time-averaged total infiltration and infiltration rates in the lower soil layer, as shown in **Figs. 1(b)** and **(c)**.

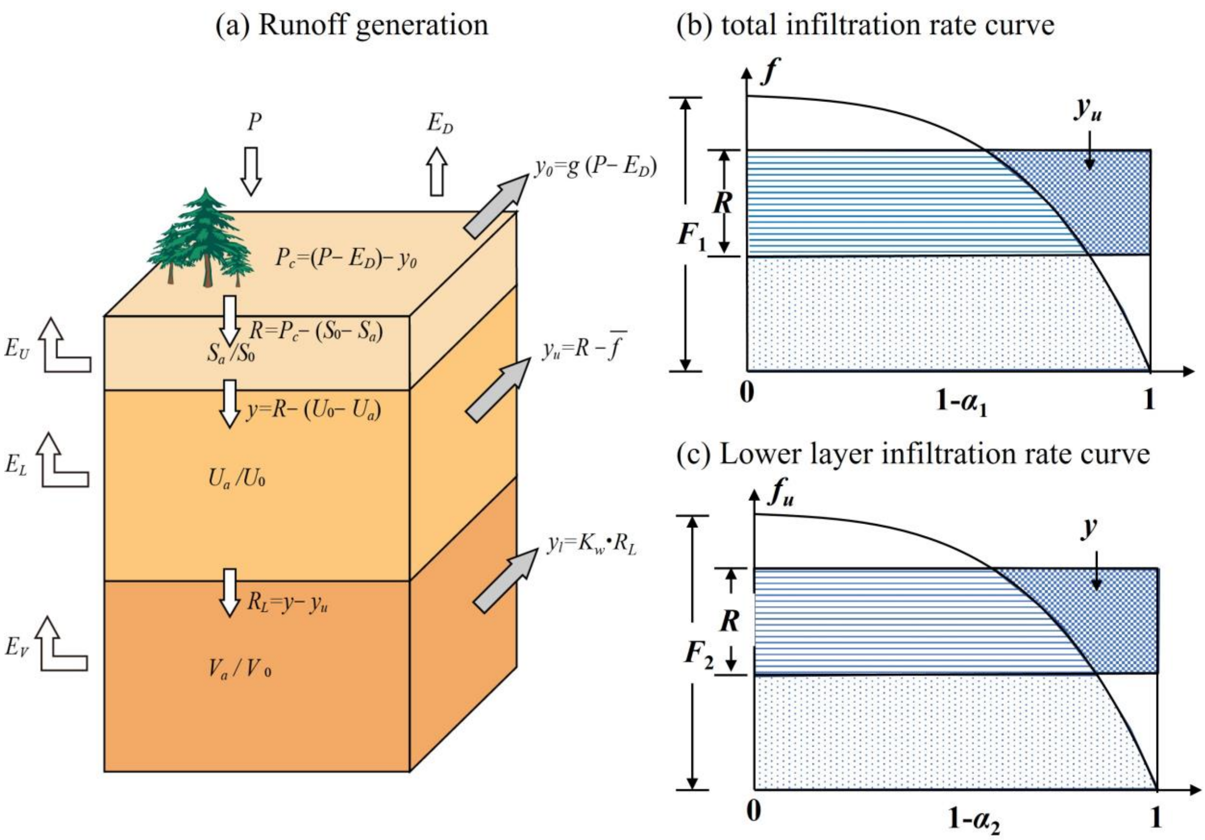

Fig. 1 The runoff generation structure of the lumped DHF model. (a) Soil generalization in three layers; (b) Total infiltration rate curve; (c) Lower layer infiltration rate curve.

Runoff includes direct runoff y_0 in impervious areas, surface runoff y_u, and groundwater runoff y_l. Direct runoff y_0 in impervious areas is:

$$PE = P - E_D \tag{1}$$

$$y_0 = g \cdot PE \tag{2}$$

where P is the precipitation, E_D is the evapotranspiration from the canopy layer, and g is the percentage of impervious area.

In semi-humid and semi-arid watersheds, the total infiltration rate f and the lower layer infiltration rate f_u are assumed to vary across the study area, as shown in **Figs. 1(b)** and **1(c)**. This formulation assumes that the total infiltration rate f and the lower layer infiltration rate f_u vary within an area and can be expressed as:

$$\alpha_1 = 1 - (1\text{-}f / F_1)^{B-1} \tag{3}$$

$$\alpha_2 = 1 - (1\text{-}f_u / F_2)^{B-1} \tag{4}$$

where α_1 is the fraction of an area for which the total infiltration rate is less than f, α_2 is the fraction of an area for which the lower layer infiltration rate is less than f_u, F_1 and F_2 are the maximum total infiltration rate and the maximum lower layer infiltration rate, respectively, and B is the shape parameter.

The complete derivation from Eqs. (3~4) to Eqs. (5~6) is given in Appendix A. Total runoff y and surface runoff y_u can be expressed as

$$y = R - \overline{f_u} \tag{5}$$

$$y_u = R - \overline{f} \tag{6}$$

where R represents the total infiltration intensity; $\overline{f}$ and $\overline{f_u}$ are the average total infiltration rate and the average lower layer infiltration rate, respectively.

The lumped DHF model calculates groundwater runoff y_l, with these equations:

$$R_L = \mathrm{y} - y_u \tag{7}$$

$$\mathrm{y}_l = K_w \times R_L \tag{8}$$

where R_L represents the infiltration intensity of the lower soil layer; K_w is the ratio of y_l to R_L. In semi-arid and arid areas, K_w=0, and thus no groundwater runoff is generated. In semi-humid and humid areas, K_w =1, and the groundwater runoff is entirely generated by the infiltration intensity R_L.

Groundwater runoff is a noteworthy component of the hydrological cycle in semi-humid and semi-arid watersheds. However, the lumped DHF model oversimplifies the generation of groundwater runoff and ignores the regulation of groundwater storage in the groundwater runoff calculation, which may result in an unreasonable allocation of runoff components (Arsenault, 2017). In the GDHF model, the generation of groundwater runoff is modified.

2.2 The GDHF model

2.2.1 GDHF model structure

The GDHF model discretizes the watershed into grid cells, assuming that surface layer interception, evapotranspiration, and infiltration calculations are performed individually for each grid cell. **Fig. 2** illustrates the structure of the GDHF model, which consists of three primary modules: runoff generation, flow routing, and reservoir regulation. The runoff generation module adopts the double-layer infiltration mechanism of the lumped DHF model to facilitate the estimation of surface runoff. To consider the dynamics of deep soil moisture, the widely used ARNO model (Todini, 1996) was employed for generating groundwater runoff. The routing module utilizes a two-parameter Gamma distributed unit hydrograph to describe the hillslope routing. Meanwhile, to address the highly non-linearity of river channel routing, a time-varying distributed unit hydrograph considering rainfall intensity is developed for river channel routing. In the reservoir module, the spatial distribution of small and medium-sized reservoirs and their storage capacity were considered in the watershed.

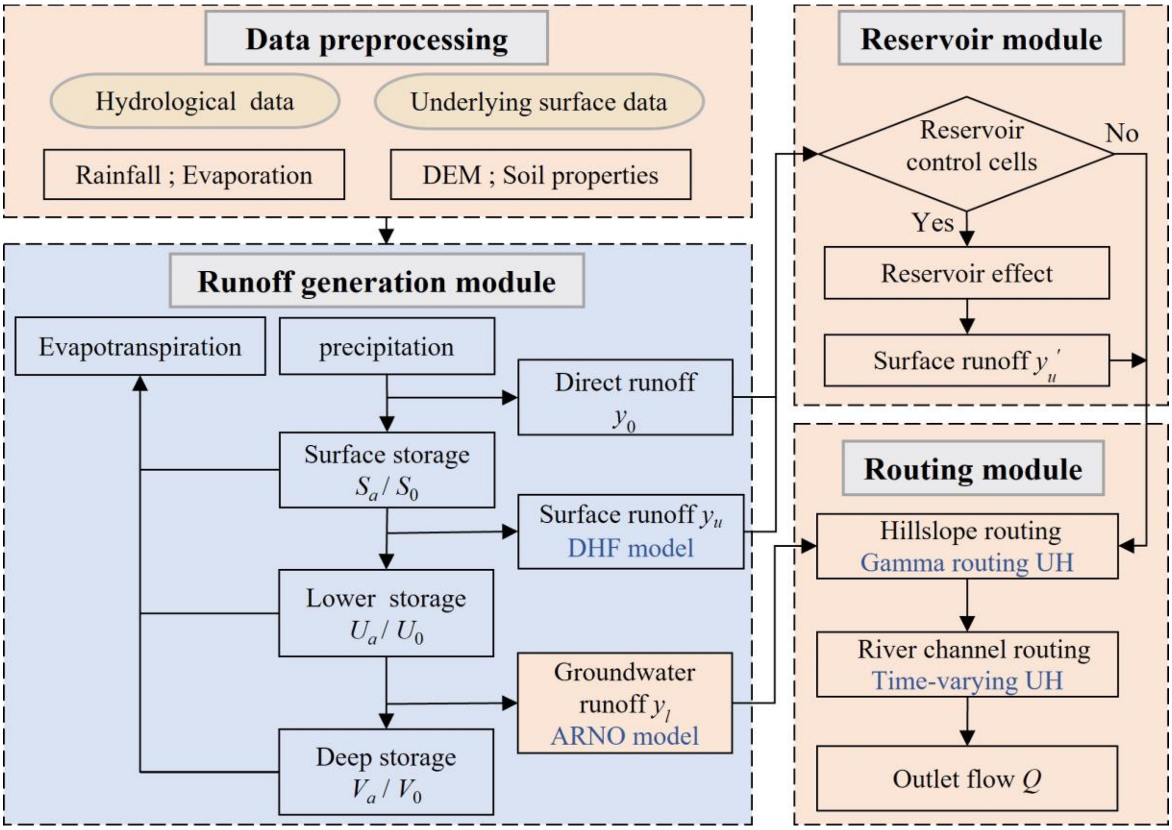

Fig. 2 Schematic diagram of the GDHF model structure, including data preprocessing, the runoff-generation module, the routing module, and the reservoir module, where the blue coverage shows the runoff generation structure of the lumped DHF model and the pink coverage shows the improved parts of the GDHF model.

(1) Runoff generation module

Compared to the lumped DHF model, the runoff generation module of the GDHF model has improved in estimating soil moisture capacity parameters and calculating groundwater runoff generation.

The soil moisture capacity is key parameters for calculating runoff generation. Previously, the lumped DHF model did not account for watershed soil types, the soil moisture capacity of each layer had to be obtained by calibration. In the GDHF model, the soil moisture capacity is determined by the soil type of each grid cell, which helps to improve the GDHF model's ability to accurately estimate the soil moisture of each grid cell. The soil properties used to calculate the soil moisture capacity include the soil moisture content fraction at the critical and wilting point. Eqs. (9-11) are used to obtain the soil moisture capacity of each layer.

$$S_0 = D_1 \times (\theta_{f,1} - \theta_{w,1}) \tag{9}$$

$$U_0 = D_2 \times (\theta_{f,2} - \theta_{w,2}) \tag{10}$$

$$V_0 = D_3 \times (\theta_{f,3} - \theta_{w,3}) \tag{11}$$

where S_0, U_0, and V_0 are the soil moisture capacity of the upper, lower, and deep layers of the soil, respectively; D_1, D_2, and D_3 are the thickness of the upper, lower, and deep layers of the soil, respectively; $\theta_{f,1}$, $\theta_{f,2}$, and $\theta_{f,3}$ are the fractional soil moisture content at the critical point of the upper, lower, and deep layers, respectively; $\theta_{w,1}$, $\theta_{w,2}$, and $\theta_{w,3}$ are the fractional soil moisture content at the wilting point of the upper, lower, and deep layers, respectively.

To rationally depict the interaction between groundwater runoff generation and deep soil moisture, the ARNO model was used for generating groundwater runoff. The ARNO model describes the vertical one-dimensional soil water movement using the Richards equation (Franchini and Pacciani, 1991), and the equation is expressed as:

$$\begin{cases} y_l = \dfrac{D_s D_m}{W_s V_0} V_a, 0 \le V_a \le W_s V_0 \\ y_l = \dfrac{D_s D_m}{W_s V_0} V_a + (D_m - \dfrac{D_s D_m}{W_s})(\dfrac{V_a - W_s V_0}{V_0 - W_s V_0})^2, V_a > W_s V_0 \end{cases} \tag{12}$$

where D_m is the maximum groundwater runoff, D_s is the ratio of D_m, and W_s is the ratio of the maximum soil moisture.

(2) Routing module

The routing simulation is categorized into hillslope routing and river routing. The hillslope routing has a short routing path and quick routing time, so the effect of rainfall intensity on the hillslope routing can be neglected. The GDHF model uses a simple two-parameter Gamma distribution unit hydrograph for hillslope routing. The shape of the unit hydrograph is controlled by the shape parameters a and the time scale parameter θ. The Gamma distribution function is calculated as

$$\gamma(t:a,\theta)=\frac{1}{\Gamma(a)\theta^{a}}t^{a-1}e^{-\frac{t}{\theta}} \tag{13}$$

where t denotes time, a is the shape parameter, and θ denotes the time scale parameter.

However, river routing is characterized by long routing paths and complex topology, resulting in a strong non-linearity of the river routing. To address the strong non-linearity of the river routing, a time-varying unit hydrograph (TVUH) considering rainfall intensity was proposed. The TVUH was developed based on the IRF-UH (Lohmann et al., 1996; Mizukami et al., 2016), which is a distributed unit hydrograph and has been widely used for daily and monthly river routing. The IRF-UH model is based on the 1-D diffusive wave equation, calculated as follows:

$$\frac{\partial q}{\partial t}=D(\frac{\partial^{2} q}{\partial x^{2}})-C(\frac{\partial q}{\partial x}) \tag{14}$$

where q is discharge, x is the location in a river channel, C indicates the wave celerity, and D indicates the diffusion coefficient.

By considering the rainfall intensity, the wave celerity C is calculated as

$$C=C_{0}(\frac{i}{i_{0}})^{k} \tag{15}$$

where C_0 is the average wave celerity of the river routing, i is the net rain intensity for the time-varying unit hydrograph of each grid cell, estimated by the average net rain intensity i_t of each grid cell, obtained by **Table 1**, i_0 is the defined net rainfall intensity corresponding to the flow velocity C_0, and k is the characteristic parameter; the value is taken as 0.4 (Kong and Guo, 2019).

Table 1. The value of net rainfall intensity i for the time-varying unit hydrograph

i_t (mm/h)	$0 < i_t \leq 10$	$10 < i_t \leq 20$	$20 < i_t \leq 30$	$30 < i_t \leq 40$	$40 < i_t \leq 50$	$i_t > 50$
i (mm/h)	5	15	25	35	45	50

The TVUH model considers the rainfall intensity, calculated as follows:

$$\frac{\partial q}{\partial t}=D(\frac{\partial^{2} q}{\partial x^{2}})-C_{0}(\frac{i}{i_{0}})^{k}(\frac{\partial q}{\partial x}) \tag{16}$$

As demonstrated in **Figs. 3(a)**, with the net rainfall intensity i changes, the shape of the TVUH calculated by Eq. (16) also changes. In **Fig. 3(b)**, with the distance from each grid cell to the watershed outlet varies, the TVUH of each grid cell is impacted by the routing path with various shapes. Therefore, the TVUH comprehensively considers the effects of the rainfall intensity and the spatial variability of geomorphic features.

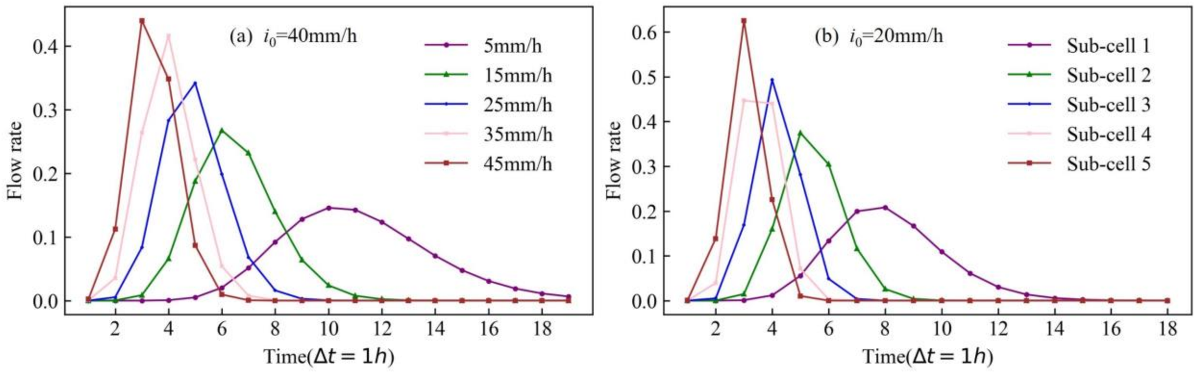

Fig. 3 Examples of TVUH consider both geographic features and rainfall intensity. (a) Shape of TVUH for different rainfall intensities. (b) Shapes of TVUH for different grid cells.

(3) Reservoir module

To consider the effect of small and medium-sized reservoirs on sub-daily flood forecasting in the absence of real-time operational data, a reservoir capacity allocation method was proposed in the GDHF model that accurately depicts their storage and discharge effects on each grid cell, as shown in **Fig. 4**. Initially, based on the spatial distribution of reservoirs, the number and locations of grid cells controlled by reservoirs were calculated. Subsequently, the utilizable capacity of each reservoir was distributed evenly to all grid cells under control. Finally, given that some grid cells are controlled by numerous reservoirs in the watershed, the utilizable storage capacity of multiple reservoirs must be added together to obtain the maximum storage capacity of each grid cell. The maximum storage capacity of each grid cell $V_{max,i}$ is calculated by

$$V_{max,i} = \sum_{j=1}^{m} \frac{1}{N_j} V_{c,j} \tag{17}$$

where $V_{max,i}$ is the maximum storage capacity of each grid cell, N_j is the number of grid cells for the j' reservoir under control, and $V_{c,j}$ is the utilizable storage of the j' reservoir.

Fig. 4(c) illustrates the results of the maximum storage capacity of each grid cell across the watershed. The grid cells are divided into two types: the grid cells affected by reservoirs and the grid cells not affected by them. By using the reservoir capacity allocation method, the

GDHF model accurately simulates the impact of the reservoir on the runoff generation and routing processes in each grid cell. The specific calculation for the reservoir module is provided in Appendix B.

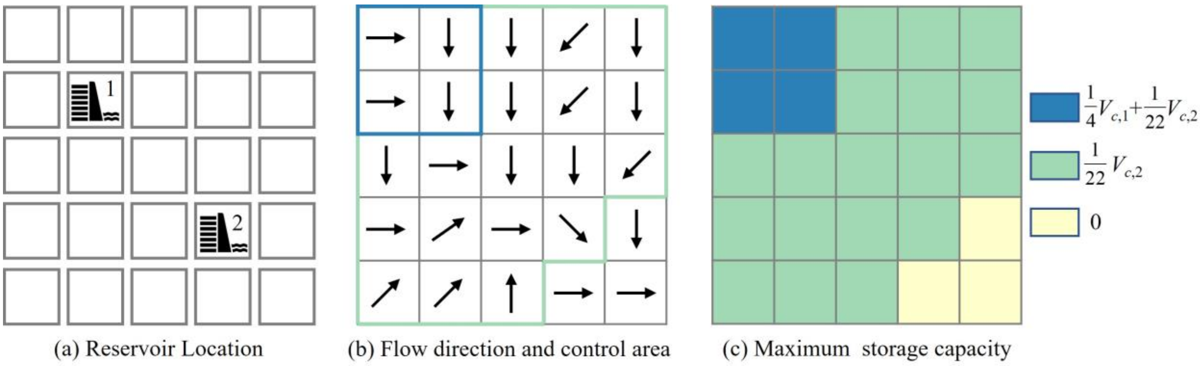

Fig. 4 Calculation flowchart of the maximum storage capacity of each grid cell

2.2.2 GDHF model parameters

Most parameters in the GDHF model have a definite physical meaning, such as soil porosity, critical water content, etc., which are obtained directly from the soil type and soil properties without calibration and are unique in each grid. The parameters of the GDHF model that need to be calibrated consist of nine soil parameters sensitive to the runoff generation process, five sensitive routing parameters that are influential on the routing processes, and three reservoir parameters. **Table 2** presents both the physical interpretation and respective reasonable ranges of the GDHF model sensitive parameters. Given only observed hydrological data at the outlet of the watershed, the model sensitivity parameters obtained from calibration are the same for all grid cells across the whole watershed.

Table 2. The physical interpretation and reasonable range of GDHF model parameters

Type	Parameters	Physical interpretation	Unit	Range
	A	Soil water storage capacity shape parameter	-	1.50-5.00
	B	Infiltration curve shape factor	-	1.00-3.00
	K_2	Curvature coefficient of the infiltration curve	-	0.20-0.90
Runoff	D_s	The ratio of D_m	-	0.01-1.00
	D_m	The maximum of groundwater runoff	mmd^{-1}	5.0-30.0
	W_s	Ratio of maximum water content in deep soil	-	0.10-1.00
	D_1	Thickness of the surface soil	mm	10-50

	D_2	Thickness of the lower soil	mm	30-100
	D_3	Thickness of the deep soil	mm	30-100
Routing	a	Shape parameter	-	0.1-3.0
	θ	Timescale parameter	h	1-24
	C_0	Wave velocity	ms^{-1}	1.0-2.5
	D	Diffusion coefficient	m^2s^{-1}	400-1500
	i_0	Net rainfall intensity	mmh^{-1}	0-50
Reservoir	m	Reservoir parameter of storage effect	-	0-1
	n	Reservoir parameter of discharge effect	-	0-1
	A_{res}	Boundary point of the storage rate	-	0-1

2.2.3 Model parameter calibration and evaluation

Conducting parameter sensitivity analysis is imperative for minimizing the computational burden for efficient calibration. The Fourier Amplitude Sensitivity Test (FAST) is a robust and computationally efficient global method for assessing parameter sensitivity in distributed hydrological models (Singh and Jha, 2021). In this study, the FAST method was used to analyze the sensitivity ranking of 17 parameters related to runoff generation, flow routing, and reservoir modules. The FAST module of SAFE toolbox software is used to calculate the first-order sensitivity index in this study (Noacco et al., 2019; Pianosi et al., 2015).

Based on the findings of the parameter sensitivity analysis, the sensitive parameters were calibrated using the NSGA-II optimization algorithm (Deb et al., 2002), which is characterized by high computational efficiency and fast convergence appropriate for dealing with high-dimensional problems. The parameter calibration is as follows: the three parameters (D_s, D_m, and W_s) of the groundwater runoff calculation are primarily determined to ensure that the simulated streamflow in the non-flood season matches the observed data as closely as possible. Then the remaining runoff generation and routing parameters that have a significant impact on the flood simulation are calibrated.

Several statistical metrics are used to evaluate the performance of hydrological models, as shown in **Table 3.** The relative error of runoff (*BIAS*) is used to assess the simulation accuracy of the runoff generation processes; the relative error of flood peak (*RPE*) and peak present time error (*PTE*) are used to assess the simulation accuracy of the routing processes. The Nash-

Sutcliffe efficiency coefficient (*NSE*) and correlation coefficient (*CC*) are used to assess the overall model simulation performance. In **Table 3**, Q_{sim} and Q_{obs} are the simulated discharge and observed discharge, respectively. T_{sp} and T_{op} are the simulated flood peak time and the observed flood peak time, respectively.

Table 3. Statistical metrics used for model calibration and evaluation

Statistical metrics	Meaning	Equation	Perfect value
NSE	Nash-Sutcliffe efficiency coefficient	$NSE = 1 - \frac{\sum(Q_{\text{sim}} - Q_{\text{obs}})^2}{\sum(Q_{\text{obs}} - \overline{Q_{\text{obs}}})^2}$	1
CC	Correlation coefficient	$CC = \frac{\sum(Q_{\text{sim}} - \overline{Q_{\text{sim}}})\sum(Q_{\text{obs}} - \overline{Q_{\text{obs}}})}{\sqrt{(Q_{\text{sim}} - \overline{Q_{\text{sim}}})^2}\sqrt{(Q_{\text{obs}} - \overline{Q_{\text{obs}}})^2}}$	1
BIAS	Relative error of runoff	$BIAS = \frac{\sum Q_{\text{sim}} - \sum Q_{\text{obs}}}{\sum Q_{\text{obs}}}$	0
RPE	Relative error of flood peak	$RPE = \frac{\max(Q_{\text{sim}}) - \max(Q_{\text{obs}})}{\max(Q_{\text{obs}})}$	0
PTE	Peak present time error	$PTE = T_{sp} - T_{op}$	0

3 Study area and Data processing

3.1. Study area

In this study, we selected eight semi-humid and semi-arid watersheds in northern China as our study areas, including Chaersen, Qinghe, Chaihe, Dahuofang, Huanren, Biliuhe, Xueye, and Laiwu watersheds. The spatial locations of rainfall stations, hydrological stations, and small and medium-sized reservoirs in these watersheds are shown in **Fig. 5**. The Dahuofang, Huanren, and Laiwu watersheds are severely impacted by small and medium-sized reservoirs, and the total capacity of reservoirs in these watersheds has accumulated to over 100 million m^3. The watersheds (a)~(f) are located in the Song-Liao Watershed, which features a typical temperate semi-humid and semi-arid monsoon climate. The Xueye and Laiwu watersheds downstream of the Yellow River exhibit a typical warm temperate semi-humid climate characteristic. **Table 4** presents the hydrological characteristics of these watersheds, including watershed area, annual average rainfall, annual average runoff depth, and runoff coefficient. The areas of the watersheds range from 427 to 10500km^2, wherein the majority receive an average annual rainfall of approximately 700 mm. The rainfall in these study watersheds is mainly concentrated in the flooding season, which transpires from June to August and accounts for over 50% of the annual rainfall. The multi-year average runoff coefficient falls in the range of 0.29-0.71.

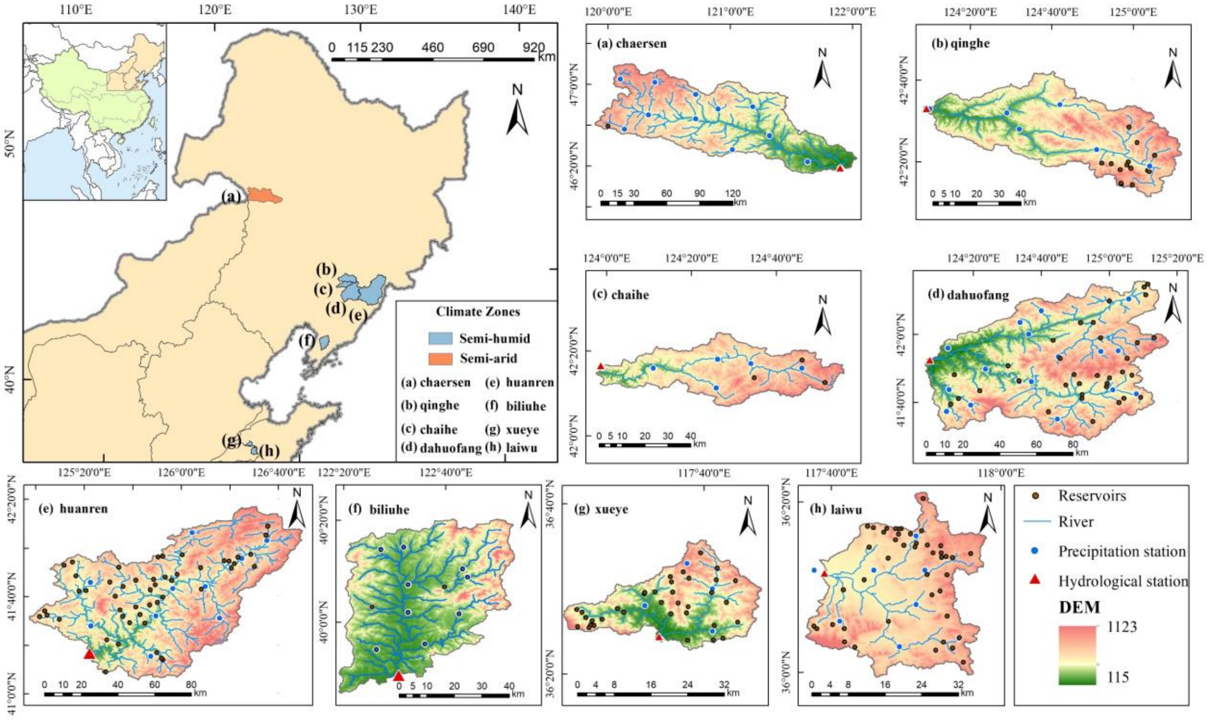

Fig. 5 Spatial location, distribution of hydrologic stations and reservoirs, river network, and DEM of the eight study watersheds. (a) Chaersen, (b) Qinghe, (c) Chaihe, (d) Dahuofang, (e) Huanren, (f) Biliuhe, (g)Xueye, and (h) Laiwu.

Table 4. Hydrological characteristics of study watersheds

Watershed	Chaersen	Qinghe	Chaihe	Dahuofang	Huanren	Biliuhe	Xueye	Laiwu
area (km^2)	7648	2389	1315	5452	10500	2085	427	751
Annual average rainfall (mm)	329.0	744.9	758.8	785.4	620.2	725.0	748.4	702.5
Annual average runoff depth (mm)	108.5	530.5	286.6	283.6	381.0	293.5	216.4	245.9
Annual average Runoff coefficient	0.33	0.71	0.38	0.36	0.61	0.40	0.29	0.35

3.2. Data processing

The GDHF modeling process requires various input data, including rainfall, evaporation, and underlying surface data, as presented in **Table 5**. Digital Elevation Model (DEM) data for the study watersheds is downloaded from the SRTM (Farr and Kobrick, 2000). Soil data is obtained from a 1km resolution soil type distribution map published by the Food and Agriculture Organization of the United Nations (FAO) (Fischer et al., 2008). Rainfall and streamflow data, as well as location and storage information for small and medium reservoirs, are obtained from the watershed authority. Rainfall data from rainfall stations was converted into grid-based rainfall data through the inverse distance weighting interpolation method (Lu and Wong, 2008). To satisfy the timeliness of flood forecasting, the time interval of flood simulation is set at 1-6h. We chose the grid resolution of the watersheds based on their area, with a grid resolution of 5 km for watersheds over 3,000 km^2 and a grid resolution of 3 km for watersheds under 3,000 km^2. The selection of grid resolution takes into account the flood forecast accuracy and computational efficiency of the GDHF model. A total of 128 flood events were collected from all study watersheds, ranked by date, with the former 60% of flood events used for calibration and the remaining 40% for validation.

Table 5. Data collection and processing of study watersheds

Data type		Resolution	Time	Data description
DEM		30 m	2018	DEM data
Soil texture		1 km	2009	Soil type and soil properties
reservoirs		/	/	Location and capacity of the reservoir
Hydrological data	Chaersen	5km/6h	1990-2015	12 flood events
	Qinghe	3km/3h	1975-2013	15 flood events
	Chaihe	3km/3h	1975-2013	12 flood events
	Dahuofang	5km/3h	1975-2019	32 flood events
	Huanren	5km/6h	2010-2017	14 flood events
	Biliuhe	3km/3h	1991-2017	21 flood events
	Xueye	3km/1h	2006-2020	12 flood events
	Laiwu	3km/1h	2006-2020	10 flood events

The GDHF modeling process focuses on the spatial discretization of the subsurface, including soil types, reservoir distribution, and river routing topology. **Fig. 6** shows the results of the spatial parameterization of the GDHF model, including (a) soil types, (b) soil properties, (c) river network topology, and (d) maximum storage capacity, using the Dahuofang watershed as an example. As shown in the spatial distribution of soil types in **Fig. 6(a)**, Halpic Luvisols (LVh) and Gleyic Luvisols (LVG) are the primary soil types in the Dahuofang watershed. **Fig. 6(b)** displays the results of the soil moisture capacity (S_0+U_0) of the surface and lower layers based on the soil type and soil thickness of each grid. The S_0+U_0 takes values in the range of

130-170 mm, showing significant spatial heterogeneity across the watershed. **Fig. 6(c)** shows the flow direction and river topology extracted from the DEM elevation data. The results of river network extraction show that there are a total of 288 grid cells that flow to the outlet of the watershed. From **Fig. 6(d)**, it can be seen that the grid cells upstream are significantly more affected by the reservoirs. Conversely, the grid cells downstream are less affected by the reservoirs.

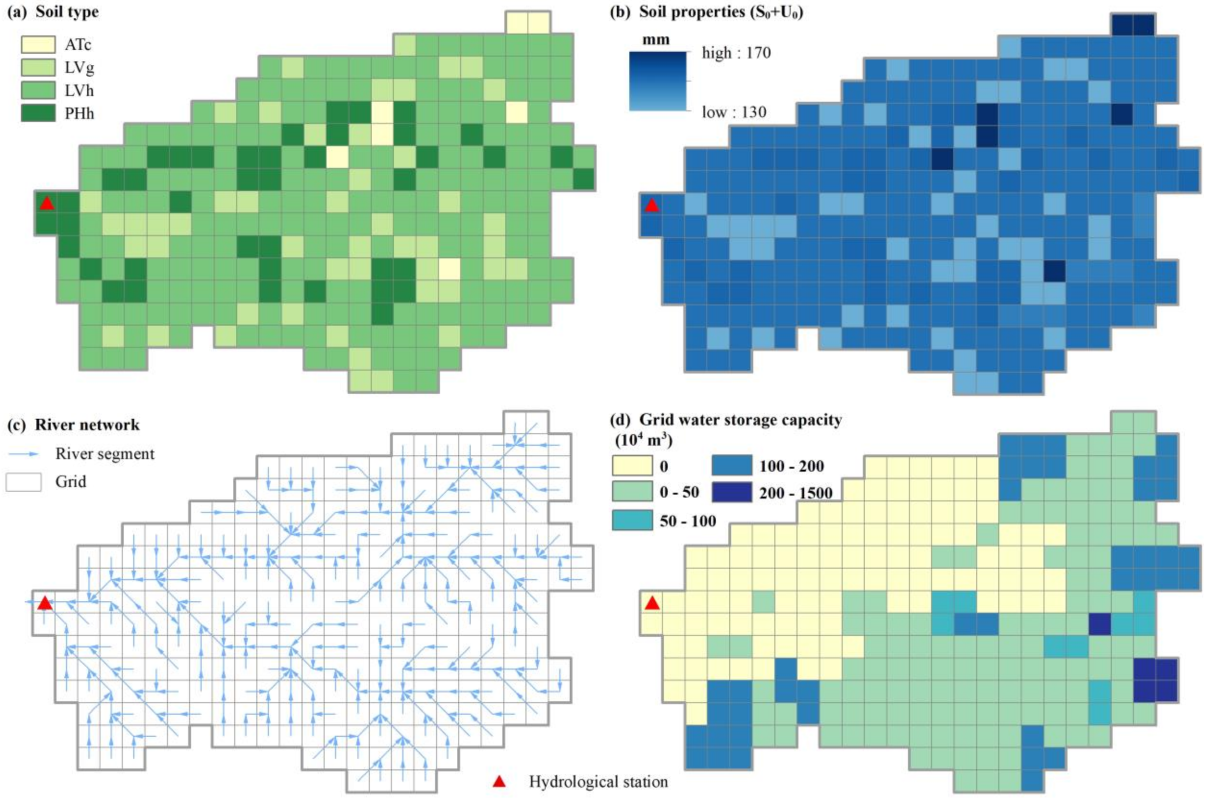

Fig. 6 Spatial distribution of (a) soil types, (b) soil properties, (c) river network and (d) grid water storage capacity in GDHF model

4 Results and Discussion

4.1 Parameter sensitivity analysis of the GDHF model

The analysis of parameter sensitivity differences in the GDHF model is carried out using the Xueye watershed as a representative area. The sensitivities of 17 parameters associated with runoff generation, flow routing, and reservoir modules in the GDHF model are evaluated. To comply with the requirements of the FAST method, we selected a total of 5798 parameter samples, and the parameter sensitivity results are presented in **Fig. 7**. The results of the FAST sensitivity index revealed the three most significant parameters that affect the output of the GDHF model across different evaluation metrics. Specifically, when the evaluation metric is *BIAS* (**Fig. 7a**), *Ares*, *B*, and D_2 are the major contributors, which explain 86.8% of the output. The evaluation of the *RPE* metric (**Fig. 7b**) reveals that *B*, D_2, and θ are responsible for a significant 53.1% of the output. For the case of *NSE* (**Fig. 7c**), the primary parameters contributing to the output are *a*, *Ares*, and θ, which explain a considerable 78.9% of the output. The main contributors to the result of the GDHF model are *D*, i_0, and *m*, explaining a significant 91.0% of the model output for the case of the *CC* indicator (**Fig. 7d**).

The FAST sensitivity analysis revealed that the sensitivity index of hydrological parameters in the GDHF model is significantly influenced by different evaluation metrics. The *BIAS*, which is closely tied to the runoff generation process, identifies the sensitive parameters A_{res}, *B*, and D_2. A_{res} is ranked first, suggesting the significant impact of small and medium-sized reservoirs on the runoff generation process. Both *RPE* and *NSE* are associated with the routing processes and jointly screen the sensitive parameter θ. In contrast, *CC* produces notably distinct outcomes from the other metrics and displays a significant variance in the sensitivity index rankings of parameters. When *CC* serves as the evaluation index, *D* and i_0 display the highest sensitivity indices for routing processes. To sum up, in the GDHF model, *Ares*, *B*, and D_2 are sensitive parameters for runoff generation, while *a*, θ, and i_0 are sensitive parameters for flow routing. Other parameters are categorized as relatively insensitive ones. A global parameter sensitivity analysis was performed on the GDHF model to obtain the parameter sensitivities and to improve computational efficiency.

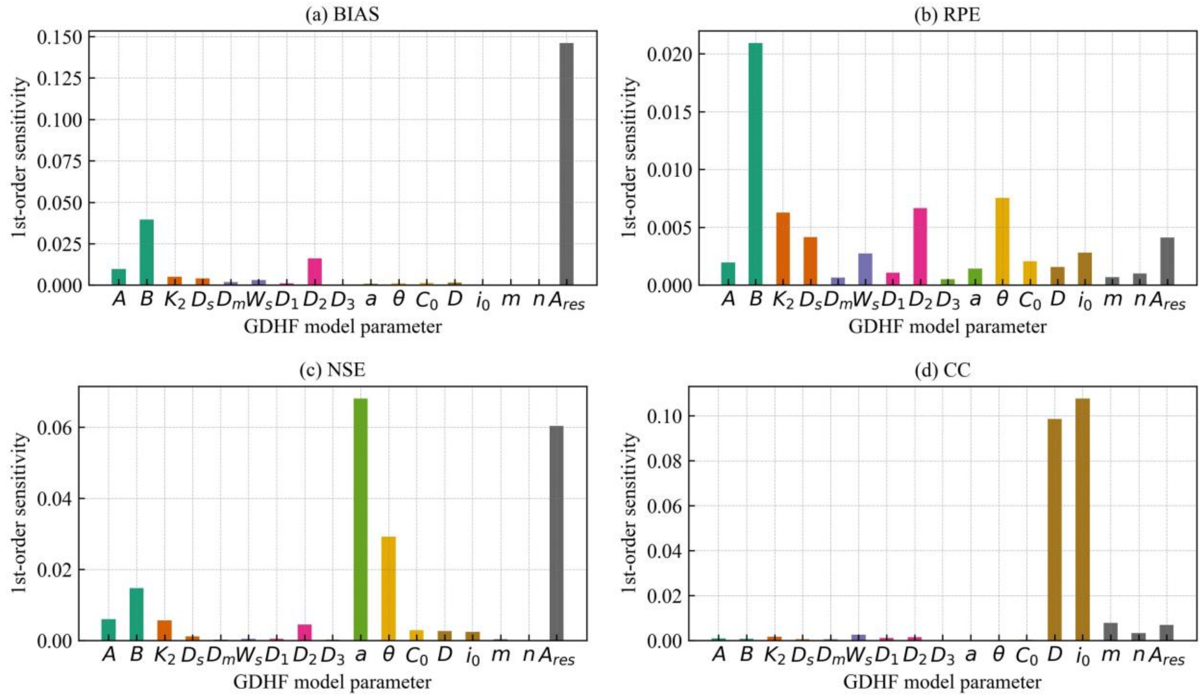

Fig. 7 GDHF model parameter sensitivity analysis results using various types of metrices

4.2 Comparison of GDHF model and lumped DHF model for overall simulation results

According to the results of the parameter sensitivity analysis, both the GDHF model and the lumped DHF model are calibrated and validated for eight study watersheds. By utilizing the evaluation metrics introduced in Section 2.2.4, the performance of the GDHF model was compared with that of the lumped DHF model. **Table 6** presents evaluation metrics for flood events during the calibration and validation periods in the study watersheds. It is worth noting that the values in **Table 6** are the average of the absolute values of the evaluation metrics for all flood events.

The results show that the GDHF model simulates an average *BIAS* and *RPE* within 10% and 15%, respectively, which significantly outperforms the lumped DHF model during the calibration and validation periods. Furthermore, the GDHF model simulated NSE values of approximately 0.80 for all study watersheds, which captured the flood characteristics of the flood event well. Although the *PTE* does not reveal a significant difference, it's simulated well in both the GDHF model and the lumped DHF model. Compared to the lumped DHF model, the GDHF model clearly obtained higher simulation accuracy for most of the flood events. This is because the GDHF model takes into account not only the spatial distribution of rainfall and subsurface but also the influences of the varying rainfall intensity and the regulation effects of reservoirs on the sub-daily flooding processes.

Table 6. Evaluation metrics in eight watersheds between the GDHF model and lumped DHF model during the calibration and validation periods

Watershed	Periods	NSE		BIAS (%)		RPE (%)		PTE (time span)	
		GDHF	DHF	GDHF	DHF	GDHF	DHF	GDHF	DHF
Xueye	Calibration	0.79	0.58	5.3	16.2	11.8	32.1	0.9	1.3
	Validation	0.87	0.81	7.9	13.0	6.3	16.5	1.0	1.8
Laiwu	Calibration	0.75	0.62	19.4	22.8	17.6	31.2	1.0	2.2
	Validation	0.81	0.63	10.8	21.9	14.9	28.3	2.0	2.8
Chaihe	Calibration	0.78	0.65	11.4	33.6	22.1	44.1	1.3	0.9
	Validation	0.81	0.74	11.0	11.6	21.7	19.2	1.6	1.2
Biliuhe	Calibration	0.81	0.76	3.9	12.8	14.1	15.7	0.9	1.0
	Validation	0.79	0.79	9.6	12.1	7.8	9.8	0.7	0.7
Qinghe	Calibration	0.81	0.67	8.6	10.8	10.3	30.8	1.3	1.2
	Validation	0.56	0.58	15.3	11.1	23.1	27.8	1.4	1.4
Dahuofang	Calibration	0.81	0.64	8.1	15.2	7.7	17.9	1.3	1.1
	Validation	0.85	0.60	6.3	15.8	11.9	18.1	0.9	1.2
Chaersen	Calibration	0.65	0.36	12.4	13.6	12.5	35.3	0.9	4.0
	Validation	0.82	0.34	3.0	28.2	9.0	25.3	0.4	1.6
Huanren	Calibration	0.79	0.54	9.0	22.6	10.0	26.1	0.4	0.9
	Validation	0.87	0.61	8.3	19.9	10.1	29.4	1.0	0.6
Average	Calibration	0.77	0.60	9.8	18.5	13.3	29.2	1.0	1.6
	Validation	0.80	0.64	9.0	16.7	13.1	21.8	1.1	1.4

4.3 Comparison of GDHF and lumped DHF model for various flood magnitudes

To evaluate the performance of the GDHF model in simulating flood events of distinctive magnitudes, a total of 128 flood events in all study watersheds have been classified into three different categories: large flood events, medium flood events, and small flood events, based on the peak magnitude of flood events. Flood events with a return period of less than 5 years are categorized as small flood events, while floods with a return period of 5-10 years are considered medium flood events. Lastly, floods with a return period of over 10 years represent large flood events.

To provide a more visual representation of the GDHF model's simulation performance at different magnitudes of flood events, **Fig. 8** represents the simulation results of the GDHF model and the lumped DHF model using box plots and scatter points. The results demonstrate that the GDHF model obtained narrower boxes and smaller simulation errors than the lumped DHF model, particularly for small and medium flood events. In semi-humid and semi-arid watersheds, most small and medium-sized flood events are characterized by small rainfall magnitudes and arid soils in the antecedent period, leading to strong non-linearity in flooding processes. By developing a reasonable runoff generation and routing structure, the GDHF model based on grid cell division efficiently simulates the non-linearity of small and medium flood events. For large floods in **Fig. 8(b)**, the *BIAS* accuracy of both models is comparable. Since the magnitude of rainfall was high and the soil was saturated in the antecedent period, the regulation effect of reservoirs was insignificant, allowing both models to simulate large flood events accurately.

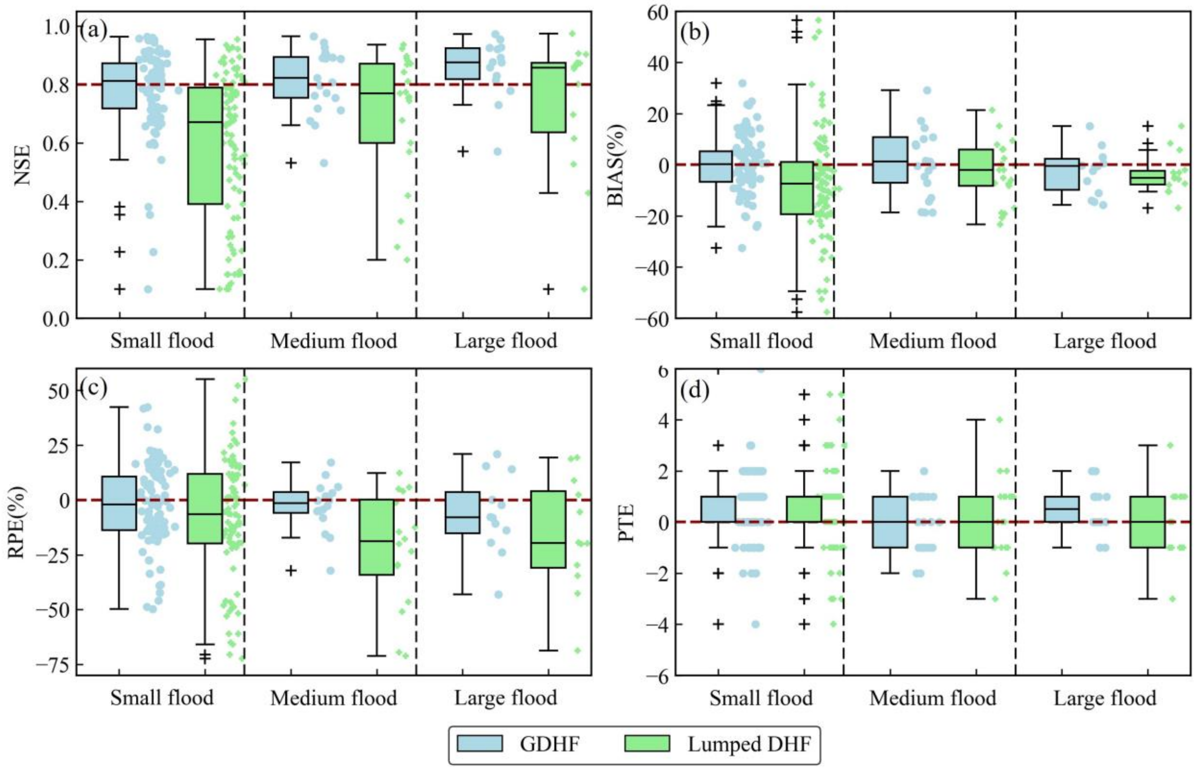

Fig. 8 Comparison of large, medium, and small flood magnitudes between the GDHF and the lumped DHF model for a total of 128 flood events in all study watersheds

4.4 Comparison of runoff generation module for GDHF model and lumped DHF model

Fig. 9 illustrates surface runoff, groundwater runoff, evaporation, and antecedent soil moisture to compare the runoff generation results of the GDHF and lumped DHF models for all flood events. The runoff generation results for each grid cell in the watershed were statistically averaged in the GDHF model. From the comparison in **Fig. 9(a)**, it can be observed that the surface runoff results obtained from the GDHF model and the DHF model are similar. The GDHF model uses the same double-layer infiltration mechanism as the lumped DHF model, so that the scatter on both sides of the 45° line shows a uniform distribution. **Fig. 9(b)** illustrates that the GDHF model significantly simulates a higher volume of groundwater runoff than the lumped DHF model for most flood events. The ARNO model is utilized in the GDHF model to calculate groundwater runoff, considering antecedent soil moisture and soil thickness. This improvement leads to more reasonable groundwater runoff calculations than the lumped DHF model.

Antecedent soil moisture is a critical hydrological variable that affects the accuracy of flood event simulation. **Fig. 9(c)** exhibits that the GDHF model's antecedent soil moisture is higher than that of the lumped DHF model for most flood events. The GDHF model uses the soil type distribution map to obtain the soil properties of each grid cell, enhancing the rationality of antecedent soil moisture calculations. **Fig. 9(d)** shows that the evaporation values for the GDHF and lumped DHF models are comparable because the evaporation mechanisms of the two models are consistent. However, the GDHF model calculates evaporation within the grid cells of watersheds, and the simulated evaporation results are more refined.

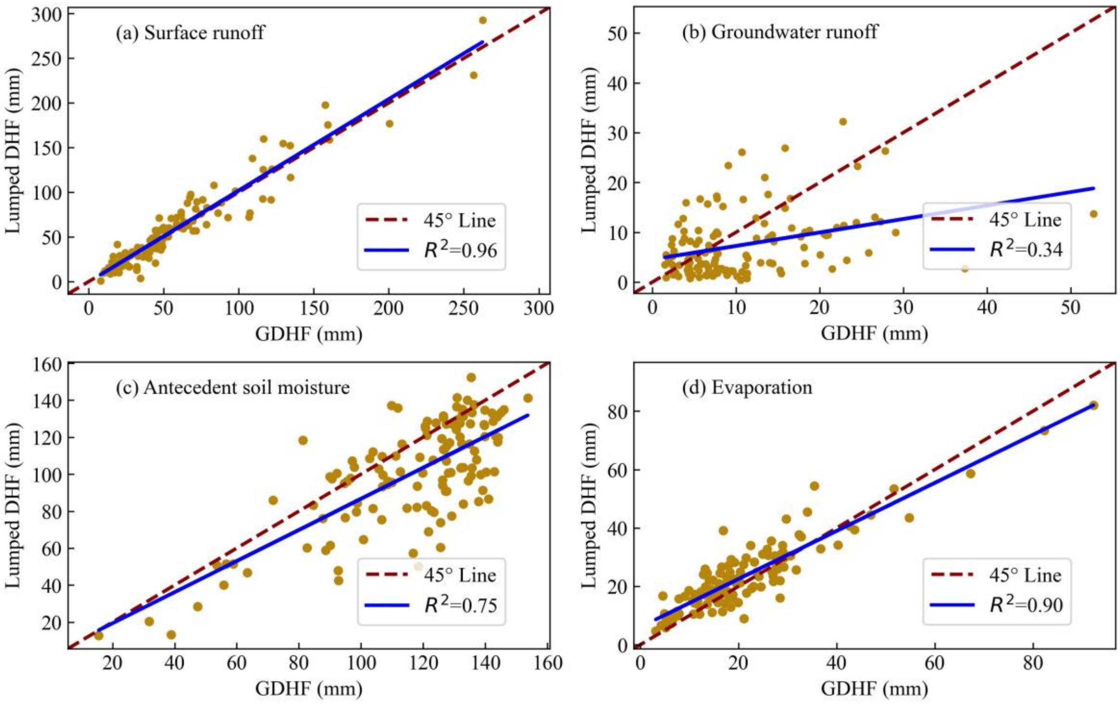

Fig. 9 Scatter plots of GDHF and lumped DHF models' runoff generation results, including (a) Surface runoff, (b) Groundwater runoff, (c) Antecedent soil moisture, and (d) evaporation

4.5 The routing results analysis of time-varying and time-invariant distributed unit hydrograph

To assess the differences between the time-varying unit hydrograph (TVUH) and the time-invariant unit hydrograph (UH), both methods were used for calculating unit hydrographs and simulating flood events of different magnitudes, respectively. The parameter calibration and validation using TVUH and UH routing methods in the Dahuofang watershed. Due to the limited length of the paper, typical flood events from all flood events are selected for in-depth analysis and presentation.

4.5.1 Large flood events

Flood event 20130816 is a typical flood in the Dahuofang watershed, with the second highest flood peak and a flood return period in excess of the 50-year return period. **Fig. 10** illustrates the difference between the TVUH and UH routing methods in the GDHF model for the large flood event 20130816. **Fig. 10(a)** represents i_{TVUH} and i_{UH}, which denote the time-varying and time-invariant net rainfall intensities of the flood event 20130816, respectively. i_{TVUH} is obtained using the values according to **Table 1**. After parameter calibration, the value of i_{UH} is 30 mm/3h. i denotes the actual net rainfall intensity. **Fig. 10(b)** illustrates the shape of TVUH and UH obtained by considering the time-varying and time-invariant net rainfall intensity, respectively. The shape of the TVUH varies with the net rainfall intensity, which is more reasonable compared with the UH. It can be seen from **Fig. 10(c)** that the simulation results of the TVUH methods are well matched with the actual flooding processes, with NSE above 0.90. However, the relative error of the flood peak simulated by the UH method exceeded 30%. This is because the TVUH method considers rainfall intensity, which is more consistent with the actual routing processes, resulting in flood simulations performing well.

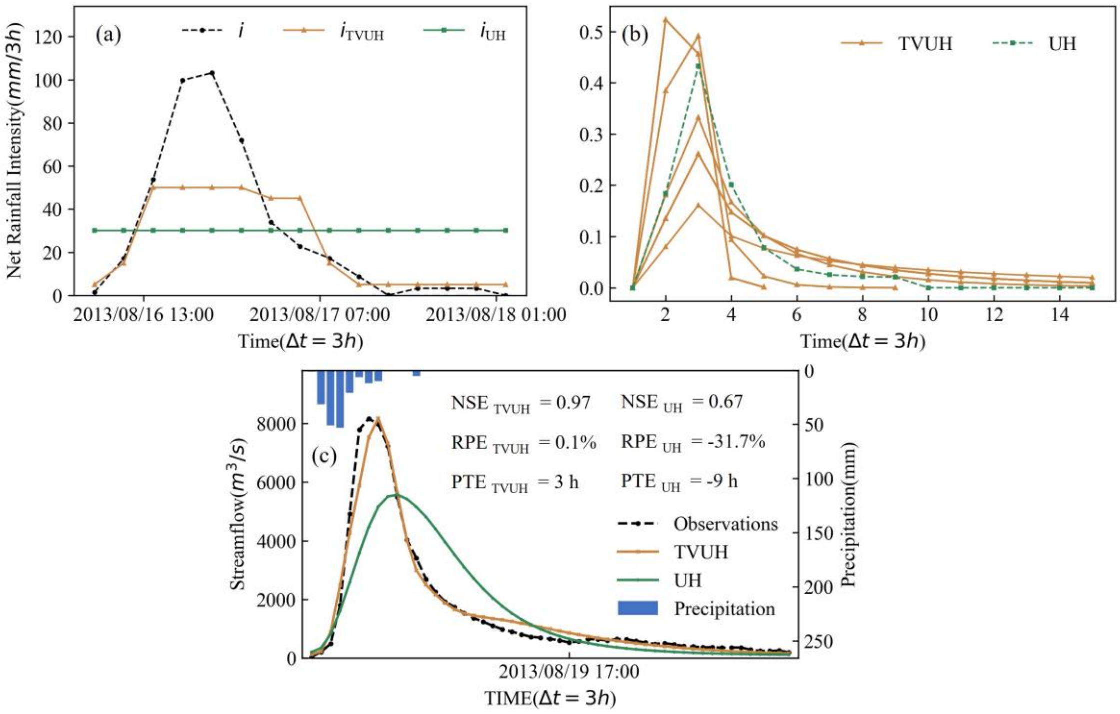

Fig. 10 Comparison of the large flood event using TVUH and UH methods in the Dahuofang watershed. (a) Net rain intensity of TVUH and UH methods. (b) The unit hydrograph results generated by the TVUH and UH methods. (c) Flood simulation results using TVUH and UH.

4.5.2 Small and medium-sized flood events

Flood event 20190811 was characterized by persistent rainfall in the watershed and was a typical multi-peak flooding process during the main flood season. **Fig. 11** presents the comparison between the TVUH and UH routing methods in the GDHF model for small and medium-sized flood events. For the flood event 20190811 depicted in **Figs. 11(a)** and **(b)**, the shape of the unit hydrograph calculated by the TVUH method is more reasonable than the UH method. **Fig. 11(c)** shows that the flooding processes by the TVUH are similar to the actual flooding processes, and the simulated flood peak is close to the actual flood peak with an RPE of only 1.6%. Conversely, the flood peak was significantly overestimated by UH, resulting in an RPE of 34.9%. This result shows that the TVUH can greatly improve the accuracy of the sub-daily routing processes for small and medium flood events.

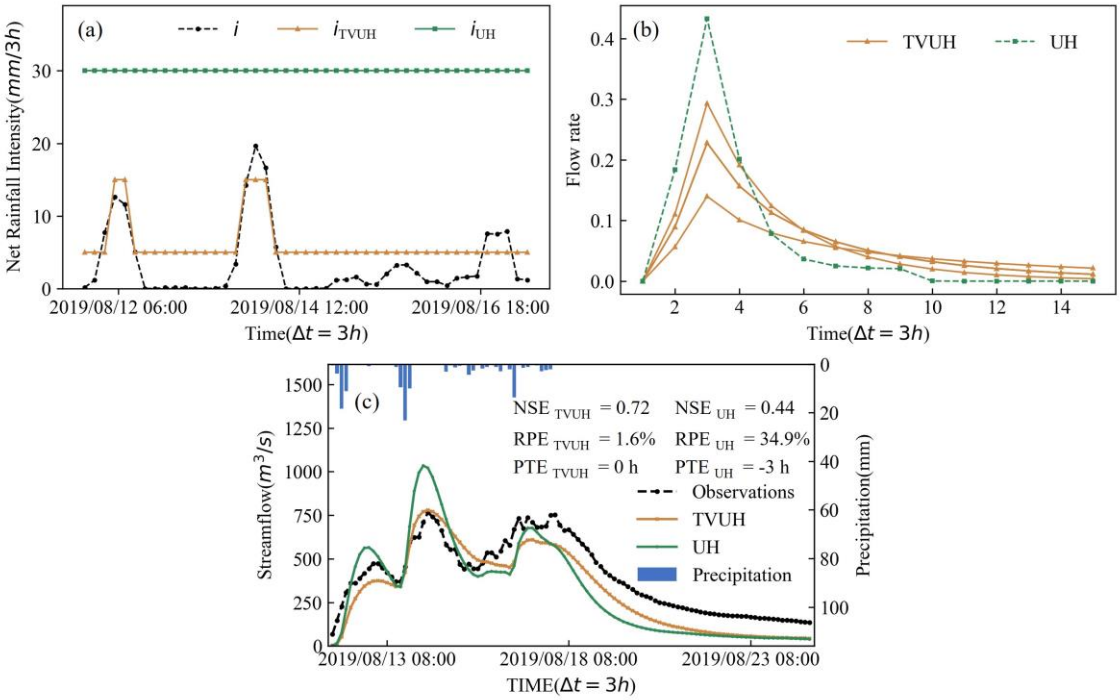

Fig. 11 Comparison of small and medium-sized flood events using TVUH and UH methods in the Dahuofang watershed. (a) Net rain intensity of TVUH and UH. (b) The unit hydrograph results generated by the TVUH and UH. (c) Flood simulation results using TVUH and UH.

4.6 The results analysis in the GDHF model with and without reservoir module

The GDHF model incorporates a reservoir method tailored for small and medium-sized reservoirs to adequately describe storage and discharge effects on each grid cell. It is worth noting that reservoir storage and discharge behavior are controlled by the location of rainfall centers, the spatial distribution of reservoirs, and the magnitude of the flood event. Typical flood events of different magnitudes were selected for in-depth analysis and presentation in the Dahuofang watershed to analyze the effect of the reservoir module.

4.6.1 Large flood events

Flood 20050812 was characterized by frequent rainfall, high antecedent soil moisture content in the watershed, and was the largest flooding process in the last decade. **Fig. 12(a)** shows that the rainfall amount of grid cells across the watershed ranged from 125-300 mm, with the rainfall center located in the middle and lower reaches. **Fig. 12(b)** illustrates that there are numerous small and medium-sized reservoirs, and the total capacity of these reservoirs exceeds 100 million m^3, which translates into a runoff depth of 30.1 mm for the whole watershed. The majority of reservoirs are situated in the upper reaches of the watershed. Conversely, in the middle and lower reaches, there are only a few reservoirs that have negligible impact on the flooding processes. The total storage of reservoirs simulated for this flood was 86.24 million m^3, which translates into a runoff depth of 16.8 mm. In **Fig. 12(c)**, the BIAS of the GDHF model with reservoir module is -4.0%, while the BIAS of the GDHF model without reservoir module is 4%. Therefore, even without considering the effect of reservoirs, the GDHF model can basically simulate the runoff amount of a large flood event.

It is worth noting that the GDHF model with the reservoir module effectively simulates the flood processes, and the flood peak error RPE is only 1.5%. On the contrary, the flood peak was overestimated by the GDHF model without the reservoir module, resulting in a 6.7% higher flood simulation result. Therefore, the routing processes simulated by the GDHF model with the reservoir module are more consistent with the actual flooding processes.

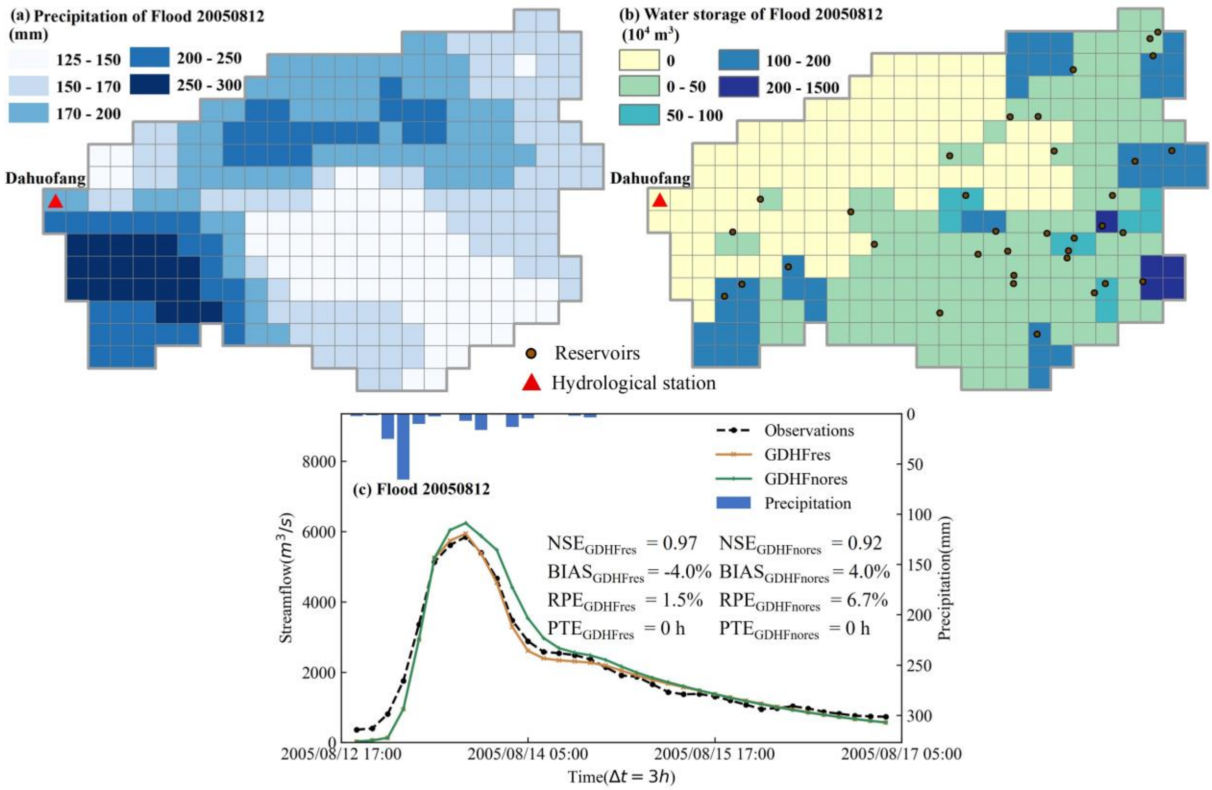

Fig. 12 Comparison of simulation results of the large flood event 20050812 with and without reservoir effects in the GDHF model. (a) Rainfall magnitude and spatial distribution of the flood event 20050812. (b) Grid total storage amounts. (c) Simulation results using the GDHF model with and without a reservoir module.

4.6.2 Small and medium-sized flood events

Flood event 19980822 was distinguished by a modest rainfall magnitude, arid antecedent soil moisture content, and typical small and multi-peak flooding in the watershed. **Fig. 13(a)** shows the spatial distribution of rainfall for the flood event 19980822. Rainfall amounts range from 50-120 mm in the grid cells, mainly concentrated on the middle and upper reaches of the watershed. **Fig. 13(b)** shows that the storage of reservoirs is obvious, and the spatial distribution of grid cell storage is very uneven for small and medium flood events with low rainfall and dry antecedent soil moisture content. The total storage of all reservoirs in this flood is 70.6 million m^3, which translates into a runoff depth of 12.9 mm. In **Fig. 13(c)**, the BIAS of the GDHF model with reservoir module is -5.7%, while the BIAS of the GDHF model without reservoir module is 16.2%. These results indicate that the GDHF model with reservoir modules can accurately simulate the actual runoff amount. Besides, the GDHF model with the reservoir module effectively simulates the flooding processes, and the RPE is only -6.4%. On the contrary, the GDHF model without the reservoir module overestimates the flood peak, and the RPE reaches 47.1%. Therefore, compared with the GDHF model without the reservoir module, the GDHF model with the reservoir module simulates both the flood amount and the flood peak of small and medium floods better.

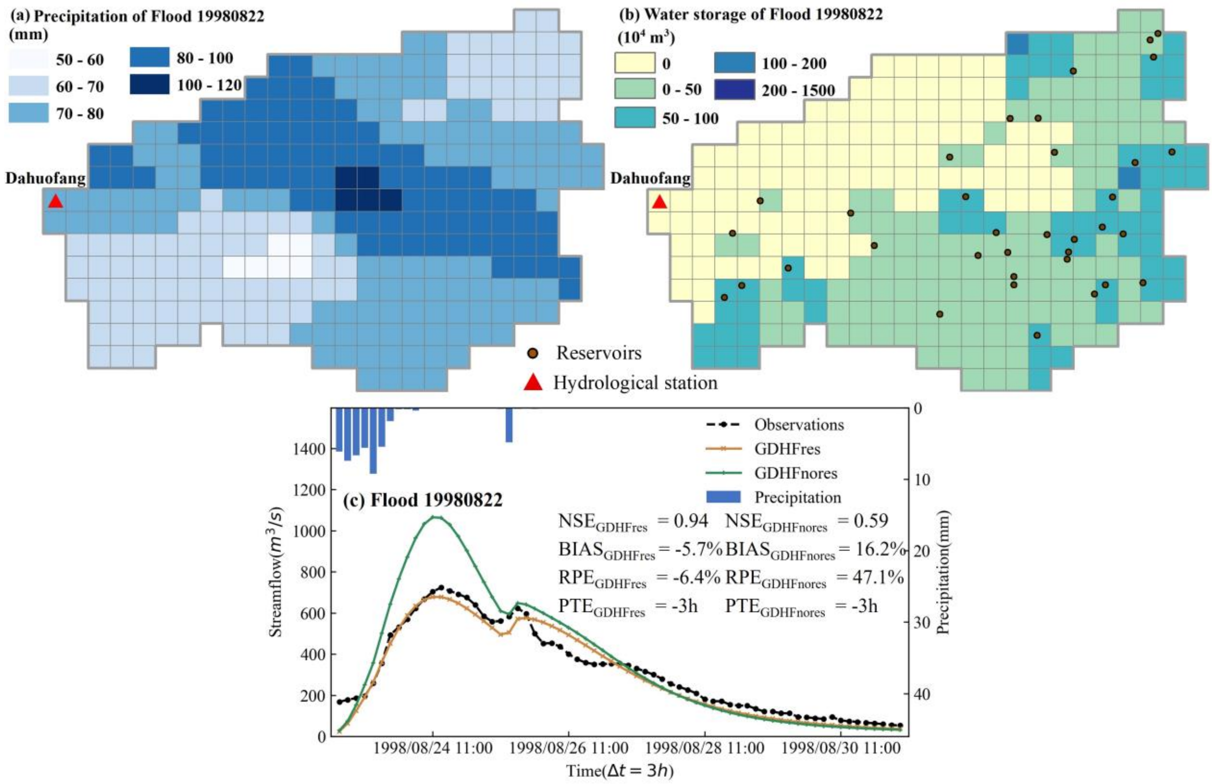

Fig. 13 Comparison of simulation results of the small and medium-sized flood event 19980822 with and without a reservoir module in the GDHF model. (a) Rainfall magnitude and spatial distribution. (b) Grid total storage amounts. (c) Simulation results using the GDHF model with and without a reservoir module.

4.7 Comparison of simulation results between the GDHF model and the VIC model

To further evaluate the difference between the GDHF model and the existing distributed models, the VIC model, which is typical in the hydrological field, was compared with the GDHF model at different time steps of 3, 6, 12, and 24 hours. The GDHF and the VIC model were calibrated at different time steps in the Dahuofang Watershed. It is worth noting that the values in **Fig. 14** are the average of the absolute values of the evaluation metrics for all flood events in the calibration and validation periods.

In **Fig. 14**, the performance of the GDHF model at different time steps is relatively steady, with the NSE basically around 0.80, the BIAS within 10%, the RPE mostly within 15%, and the PTE less than 1.0. However, for the VIC model, the simulation performance changes significantly when the time step is varied. When the time step is 24h, the evaluation metrics of the VIC model are significantly better than the sub-daily scale. Generally, the GDHF outperforms the VIC model for the simulation of the runoff generation and routing processes in all time steps. Consequently, the performance of the distributed model in simulating sub-daily flood events depends on its ability to generalize the non-linearity of the hydrological processes.

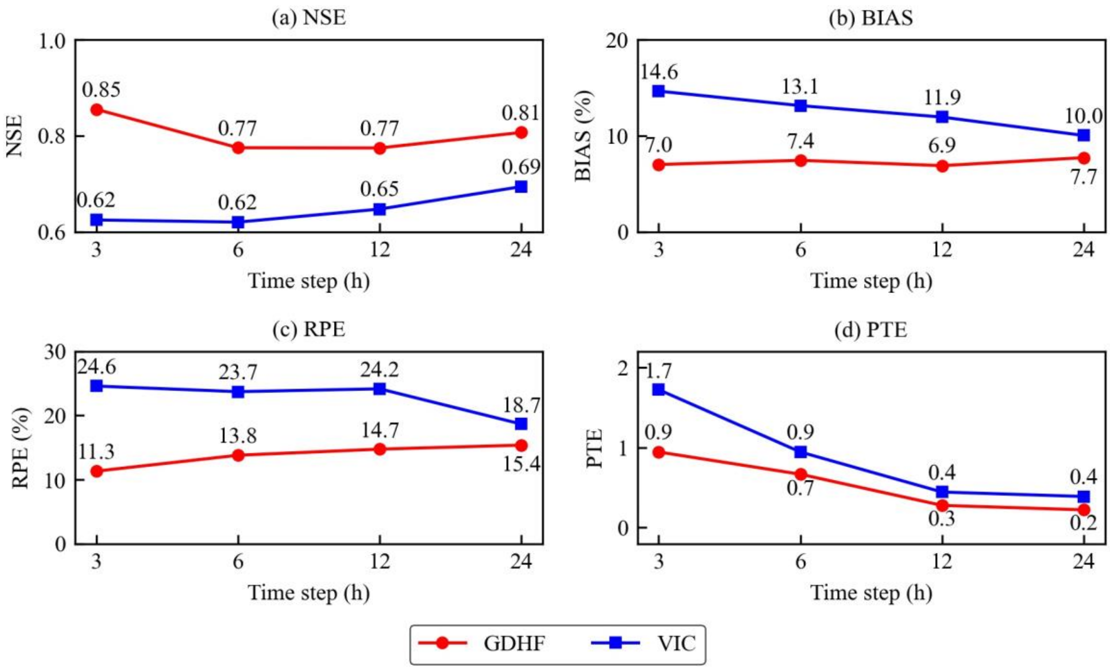

Fig. 14 Comparison of simulation results between the GDHF model and the VIC model at different time steps of 3h, 6h, 12h, and 24h in the Dahuofang watershed.

Fig. 15 presents the simulation results of the GDHF model and the VIC model at the 3h time step. Both the GDHF and the VIC model are able to capture the flooding processes at the 3h time step well. However, in terms of simulating flood volume and flood peak, the GDHF model is significantly superior to the VIC model. For flood events with a flood peak magnitude below 2000 m^3/s, these are characterized by significant effects of varying intensity and reservoirs regulation. The GDHF model adequately takes into account the non-linearity of sub-daily hydrological processes by incorporating the effects of the rainfall intensity and the reservoir's storage and discharge behavior on the flooding processes.

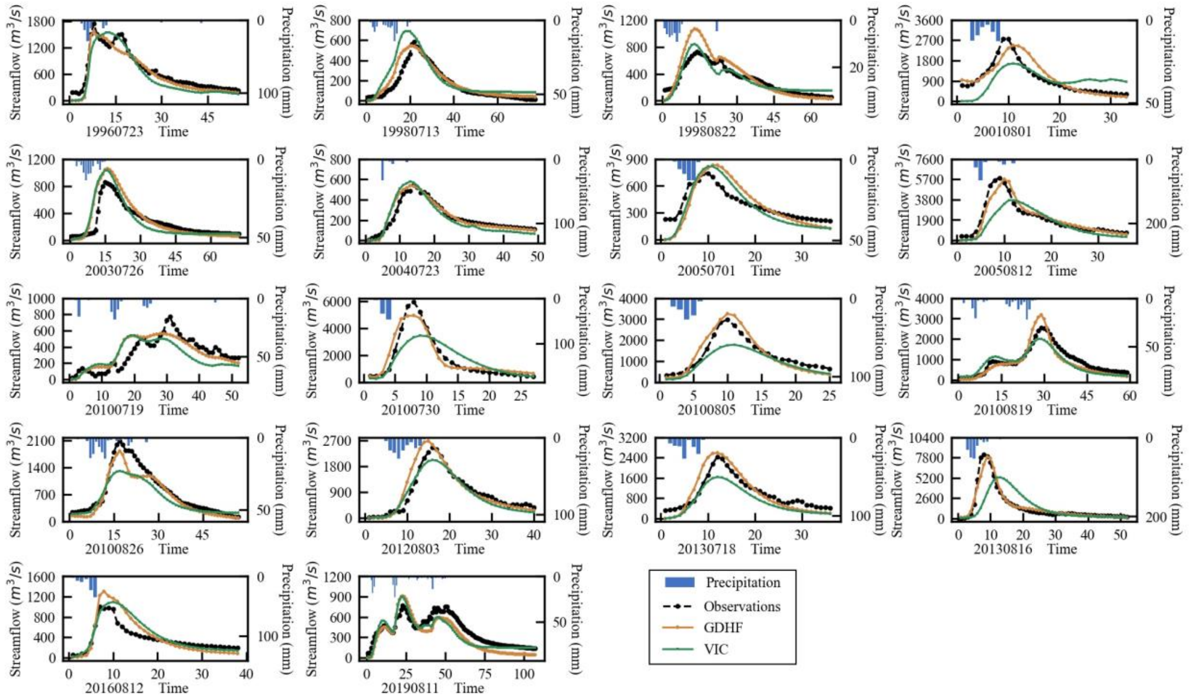

Fig. 15 Comparison of simulation results between the GDHF and the VIC model during the calibration and validation periods at the 3h time step.

5 Conclusions

To improve the comprehension of the spatiotemporal variability of sub-daily hydrological processes in semi-humid and semi-arid watersheds, this study proposes a distributed hydrological framework (GDHF) as a tool for simulating sub-daily flood events. The GDHF model was evaluated in eight representative watersheds in northern China and compared with the lumped DHF model and VIC model. The study's main conclusions are summed up as follows:

(1) The GDHF model accounts for the spatial and temporal distribution of hydrological features. The GDHF model obtained mean evaluation metric values of 0.80, 9.2%, 13.0%, and 1.05 for NSE, BIAS, RPE, and PTE, respectively. The results indicate that the GDHF model

outperformed the lumped DHF model in simulating sub-daily flood events because the model adequately accounted for the spatial and temporal distribution of hydrological features.

(2) In comparison to the traditional time-invariant distributed unit hydrograph, this study proposes a time-varying distributed unit hydrograph based on the IRF-UH method, which considers the time-varying rainfall intensity. The simulation accuracy of flood peaks was significantly improved, especially for small and medium flood events.

(3) Considering the effect of storage and discharge behavior on the natural flooding processes of the watershed, the simulation performance of flood events is significantly enhanced without relying on real-time reservoir operation data.

(4) Assessing the differences between the GDHF model and the VIC model, the performance of the GDHF model is comparable to that of the VIC model at the 24h time step. However, at sub-daily time steps, the GDHF model performs significantly better than the VIC model, especially for the 3h time step.

Acknowledgements

We are grateful for the support received as part of the projects funded by the National Natural Science Foundation of China (nos. 51925902, 52179006).

Authors' Contributions Xiaoyang Li: Conceptualization, Methodology and Writing. **Lei Ye:** Methodology, Writing and Funding acquisition. **Xuezhi Gu:** Reviewing. **Jinggang Chu:** Data analysis and reviewing. **Jin Wang:** Software and Data Curation. **Chi Zhang:** Funding acquisition and reviewing. **Huicheng Zhou:** Funding acquisition and Resources.

Declarations

Ethical Approval Not applicable.

Consent to Participate Not applicable.

Consent to Publish Not applicable.

Competing Interest The authors declare that they have no conflict of interest to this work.

Appendix A

We describe in detail the formulae for the calculation of surface runoff and groundwater runoff. The process of calculating surface runoff begins by determining the rainfall intensity (P_c). This is accomplished by subtracting the evapotranspiration (E_D) and the direct runoff (y_0) from the total rainfall (P).

$$P_c = (P - E) - y_0 \tag{18}$$

Then, the lumped DHF model calculates the infiltration intensity R by subtracting the surface water deficit (S_0-S_a) from the net rainfall intensity P_c. The lumped DHF model uses distribution curves to describe the spatial distribution of the storage capacity S_m at each point in the surface layer over the watershed.

When $S_m + P_c \le AS_0$,

$$R = P_c - \left(S_0 - S_a\right) + S_0\left(1 - \frac{(S_m + P_c)}{AS_0}\right)^A \tag{19}$$

where

$$S_m = AS_0\left[1 - \left(1 - \frac{S_a}{S_0}\right)^{\frac{1}{A}}\right] \tag{20}$$

When $S_m + P_c > AS_0$,

$$R = P_c - \left(S_0 - S_a\right) \tag{21}$$

The average total infiltration rate of the watershed at the current time $\overline{f}$ is expressed as

When $R + Z_1 D_n \le Z_1 BD_0$,

$$\overline{f} = Z_1 D_0\left(1 - \frac{U_a}{U_0}\right)^{\frac{U_0}{D_0}} - Z_1 D_0\left(1 - \frac{(Z_1 D_n + R)}{Z_1 BD_0}\right)^B \tag{22}$$

When $R + Z_1 D_n > Z_1 BD_0$,

$$\overline{f} = Z_1 D_0\left(1 - \frac{U_a}{U_0}\right)^{\frac{U_0}{D_0}} \tag{23}$$

where,

$$D_n = BD_0\left[1 - \left(1 - \frac{U_a}{U_0}\right)^{\frac{U_0}{BD_0}}\right] \tag{24}$$

$$Z_1 = 1 - e^{\frac{-k_2 \Delta t U_0}{D_0}} \tag{25}$$

where D_n is the value of the vertical coordinate corresponding to D_0, Z_1, a parameter related to rain intensity.

The average lower layer infiltration rate of the watershed at the current time $\overline{f_u}$ is expressed as

When $R + Z_2 U_n \le Z_2 B U_0$,

$$\overline{f_u} = Z_2(U_0 - U_a) - Z_2 U_0 (1 - \frac{(Z_2 U_n + R)}{Z_2 B U_0})^B \tag{26}$$

When $R + Z_2 U_n > Z_2 B U_0$,

$$\overline{f_u} = Z_2(U_0 - U_a) \tag{27}$$

where,

$$U_n = B U_0 [1 - (1 - \frac{U_a}{U_0})^{\frac{1}{B}}] \tag{28}$$

$$Z_2 = 1 - e^{-k_2 \Delta t} \tag{29}$$

where U_n is the value of the vertical coordinate corresponding to U_0, Z_2, a parameter related to rain intensity.

Appendix B

We describe in detail the calculation of the reservoir module. This method can reflect the storage and discharge patterns of reservoirs, leading to more precise flood forecasting schemes. Virtual reservoirs are created to represent the grid cells affected by reservoirs. The initial storage volume of each virtual reservoir is

$$V_b = ((S_a + U_a) / (S_0 + U_0))^{0.4} \cdot \Delta R \tag{30}$$

where V_b is the initial storage volume of the virtual reservoir before flooding.

The horizontal axis k denotes the runoff storage or discharge rate. Since most small to medium-sized reservoirs lack sluice gates, it is presumed that the boundary point of the storage rate A represents the transition point between storage and discharge effects.

When the storage rate V_b/V_{max} is smaller than A, reservoirs exert their influence in the form of storage, while when the storage rate V_b/V_{max} is larger than A, reservoirs discharge water.

$$k = \begin{cases} ((A_{res} - V_b / V_{max}) / A_{res})^m & V_b / V_{max} \le A_{res} \\ ((V_b / V_{max} - A_{res}) / (1 - A_{res}))^n & V_b / V_{max} > A_{res} \end{cases} \tag{31}$$

where the parameters A_{res}, m, and n are obtained by model calibration.

Then, the simulated runoff y_t' using the reservoir module obtained by the GDHF model is calculated as

$$y_t^{'} = \begin{cases} (1-k)\times y_t & V_b / V_{max} \le A_{res} \\ (1+k)\times y_t & V_b / V_{max} > A_{res} \end{cases} \quad (32)$$

where t is time and y_t is the total runoff.

References

Arsenault, R., 2017. HMETS—A simple and efficient hydrology model for teaching hydrological modelling, flow forecasting and climate change impacts.

Chang, C. et al., 2019. A model-aided satellite-altimetry-based flood forecasting system for the Mekong River. Environmental Modelling & Software, 112: 112-127. https://doi.org/10.1016/j.envsoft.2018.11.017

Chao, L., Zhang, K., Li, Z., Wang, J., Yao, C., Li, Q., 2019. Applicability assessment of the CASCade Two Dimensional SEDiment (CASC2D-SED) distributed hydrological model for flood forecasting across four typical medium and small watersheds in China. Journal of Flood Risk Management, 12, e12518. https://doi.org/10.1111/jfr3.12518

Clark, M. P., Kavetski, D., Fenicia, F., 2011. Pursuing the method of multiple working hypotheses for hydrological modeling. Water Resources Research, 47(9). https://doi.org/10.1029/2010WR009827

Deb, K., Pratap, A., Agarwal, S. and Meyarivan, T., 2002. A fast and elitist multiobjective genetic algorithm: NSGA-II. IEEE transactions on evolutionary computation, 6(2): 182-197. https://doi.org/10.1109/4235.996017

Devia, G.K., Ganasri, B.P. and Dwarakish, G.S., 2015a. A Review on Hydrological Models. Aquatic Procedia, 4: 1001-1007. https://doi.org/10.1016/j.aqpro.2015.02.126

Fanzhe, Kong., Liang, G., 2019. A method of deriving time- variant distributed unit hydrograph. Advances in Water Science, 30(4), 477-484. Chinese.

Farr, T.G. and Kobrick, M., 2000. Shuttle radar topography mission produces a wealth of data. Eos, Transactions American Geophysical Union, 81(48): 583.

Fischer, G. et al., 2008. Global Agro-ecological Zones Assessment for Agriculture.

Franchini, M., Pacciani, M., 1991. Comparative analysis of several conceptual rainfall-runoff models. Journal of hydrology, 122(1-4), 161-219. https://doi.org/10.1016/0022-1694(91)90178-K

Granit, J., 2014. Delivering Global Environmental Benefits for Sustainable Development: Report to the 5th GEF Assembly.

Hapuarachchi, H. A. P., Wang, Q. J., Pagano, T. C., 2011. A review of advances in flash flood forecasting. Hydrological processes, 25(18), 2771-2784. https://doi.org/10.1002/hyp.8040

He, B., Huang, X., Ma, M., Chang, Q., Tu, Y., Li, Q., ... Hong, Y., 2018. Analysis of flash flood disaster characteristics in China from 2011 to 2015. Natural Hazards, 90, 407-420. https://doi.org/10.1007/s11069-017-3052-7

Huo, W., Li, Z., Zhang, K., Wang, J., Yao, C., 2020. GA-PIC: An improved Green-Ampt rainfall-runoff model with a physically based infiltration distribution curve for semi-arid basins. Journal of Hydrology, 586, 124900. https://doi.org/10.1016/j.jhydrol.2020.124900

Khaing, Z. M., Zhang, K., Sawano, H., Shrestha, B. B., Sayama, T., Nakamura, K., 2019. Flood hazard mapping and assessment in data-scarce Nyaungdon area, Myanmar. PLoS One, 14(11), e0224558. https://doi.org/10.1371/journal.pone.0224558

Lee, K.T., CHEN, N. and CHUNG, Y., 2010. Derivation of variable IUH corresponding to time-varying rainfall intensity during storms. Hydrological Sciences Journal, 53(2): 323-337. https://doi.org/10.1623/hysj.53.2.323

Liu, A., Wang, B., 1984. Application on Microcomputer of DHF model. Journal of Dalian University of Technology, 23(3), 27-28. Chinese.

Liu, Y. et al., 2020. A hybrid runoff generation modelling framework based on spatial combination of three runoff generation schemes for semi-humid and semi-arid watersheds. Journal of Hydrology, 590: 125440. https://doi.org/10.1016/j.jhydrol.2020.125440

Lohmann, D. A. G., Nolte-Holube, R. A. L. P. H., Raschke, E., 1996. A large-scale horizontal routing model to be coupled to land surface parametrization schemes. Tellus A, 48(5), 708-721. https://doi.org/10.1034/j.1600-0870.1996.t01-3-00009.x

Lu, G.Y. and Wong, D.W., 2008. An adaptive inverse-distance weighting spatial interpolation technique. Computers & Geosciences, 34(9): 1044-1055. https://doi.org/10.1016/j.cageo.2007.07.010

Meng, W., Peng, Y. and Liang, G., 2012. Application of DHF Model in Flood Forecasting for Shifosi Basin. South to-North Water Diversion and Water Science &. Technology, 10(2): 5. Chinese.

Mizukami, N., Clark, M. P., Sampson, K., Nijssen, B., Mao, Y., McMillan, H., ... Brekke, L. D., 2016. mizuRoute version 1: a river network routing tool for a continental domain water resources applications. Geoscientific Model Development, 9(6), 2223-2238. https://doi.org/10.5194/gmd-9-2223-2016

Noacco, V., Sarrazin, F., Pianosi, F. and Wagener, T., 2019. Matlab/R workflows to assess critical choices in Global Sensitivity Analysis using the SAFE toolbox. MethodsX, 6: 2258-2280. https://doi.org/10.1016/j.mex.2019.09.033

Paul, P.K., Kumari, N., Panigrahi, N., Mishra, A. and Singh, R., 2018. Implementation of cell-to-cell routing scheme in a large scale conceptual hydrological model. Environmental Modelling & Software, 101: 23-33. https://doi.org/10.1016/j.envsoft.2017.12.003

Payan, J. L., Perrin, C., Andréassian, V., Michel, C., 2008. How can man-made water reservoirs be accounted for in a lumped rainfall-runoff model?. Water Resources Research, 44(3). https://doi.org/10.1029/2007WR005971

Peng, Y., Sun, X., Zhang, X., Zhou, H., Zhang, Z., 2017. A flood forecasting model that considers the impact of hydraulic projects by the simulations of the aggregate reservoir's retaining and discharging. Water Resources Management, 31, 1031-1045. https://doi.org/10.1007/s11269-016-1562-9

Pianosi, F., Sarrazin, F. and Wagener, T., 2015. A Matlab toolbox for Global Sensitivity Analysis. Environmental Modelling & Software, 70: 80-85. https://doi.org/10.1016/j.envsoft.2015.04.009

Singh, A. and Jha, S.K., 2021. Identification of sensitive parameters in daily and monthly hydrological simulations in small to large catchments in Central India. Journal of Hydrology, 601: 126632. https://doi.org/10.1016/j.jhydrol.2021.126632

Sivakumar, B. and Singh, V.P., 2012. Hydrologic system complexity and nonlinear dynamic concepts for a catchment classification framework. Hydrology and Earth System Sciences, 16(11): 4119-4131. https://doi.org/10.5194/hess-16-4119-2012

Tian, J. et al., 2020. A coupled atmospheric–hydrologic modeling system with variable grid sizes for rainfall–runoff simulation in semi-humid and semi-arid watersheds: how does the coupling scale affects the results? Hydrology and Earth System Sciences, 24(8): 3933-3949. https://doi.org/10.5194/hess-24-3933-2020

Todini, E., 1996. The ARNO rainfall—runoff model. Journal of hydrology, 175(1-4), 339-382. https://doi.org/10.1016/S0022-1694(96)80016-3

Werkhoven, K., Wagener, T., Reed, P. and Tang, Y., 2008. Characterization of watershed model behavior across a hydroclimatic gradient. Water Resources Research, 44(1). https://doi.org/10.1029/2007WR006271

Wheater, H., Sorooshian, S., Sharma, K. D. (Eds.)., 2007. Hydrological modelling in arid and semi-arid areas. Cambridge University Press.

Woods, R., Rowe, L., 1996. The changing spatial variability of subsurface flow across a hillside. Journal of Hydrology (New Zealand), 35(1), 51–86. http://www.jstor.org/stable/43944761

Yang, W., Chen, L., Chen, X., Chen, H., 2022. Sub-daily precipitation-streamflow modelling of the karst-dominated basin using an improved grid-based distributed Xinanjiang hydrological model. Journal of Hydrology: Regional Studies, 42, 101125. https://doi.org/10.1016/j.ejrh.2022.101125

Yao, C., Li, Z. J., Bao, H. J., Yu, Z. B., 2009. Application of a developed Grid-Xinanjiang model to Chinese watersheds for flood forecasting purpose. Journal of Hydrologic Engineering, 14(9), 923-934. https://doi.org/10.1061/(ASCE)HE.1943-5584.0000067

Yi, B., Chen, L., Zhang, H., Singh, V. P., Jiang, P., Liu, Y., ... Qiu, H., 2022. A time-varying distributed unit hydrograph method considering soil moisture. Hydrology and Earth System Sciences, 26(20), 5269-5289. https://doi.org/10.5194/hess-26-5269-2022

Zang, S., Li, Z., Zhang, K., Yao, C., Liu, Z., Wang, J., ... Wang, S., 2021. Improving the flood prediction capability of the Xin'anjiang model by formulating a new physics-based routing framework and a key routing parameter estimation method. Journal of Hydrology, 603, 126867. https://doi.org/10.1016/j.jhydrol.2021.126867

Zhang, C., Peng, Y., Chu, J., Shoemaker, C. A., Zhang, A., 2012. Integrated hydrological modelling of small-and medium-sized water storages with application to the upper

Fengman Reservoir Basin of China. Hydrology and Earth System Sciences, 16(11), 4033-4047. https://doi.org/10.5194/hess-16-4033-2012

Zhang, J. T., Li, Z., 1999. A Study on demarcation indexes between sub humid and semiarid sectors in China. Progress in Geograpgy, 18, 230-237. Chinese.

Zhao, G., Gao, H., Naz, B.S., Kao, S. and Voisin, N., 2016. Integrating a reservoir regulation scheme into a spatially distributed hydrological model. Advances in Water Resources, 98: 16-31. https://doi.org/10.1016/j.advwatres.2016.10.014